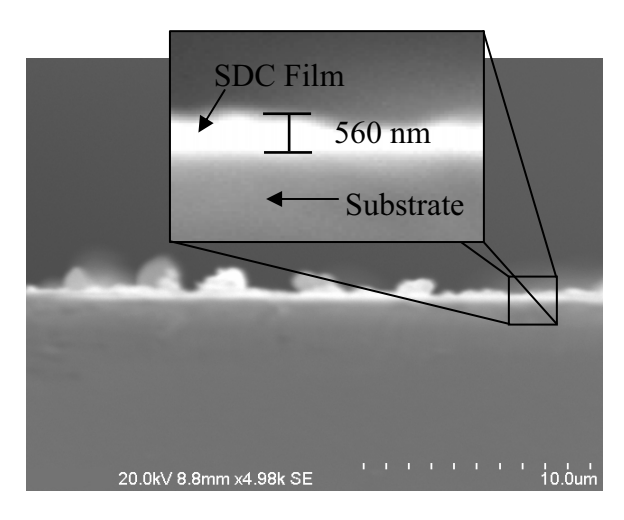
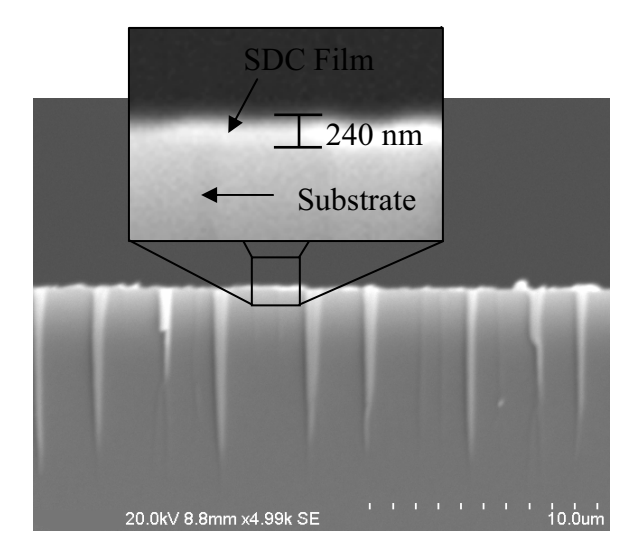


(a)



**(b)** 



(c)

Figure 7. (Ksapabutr et al.)

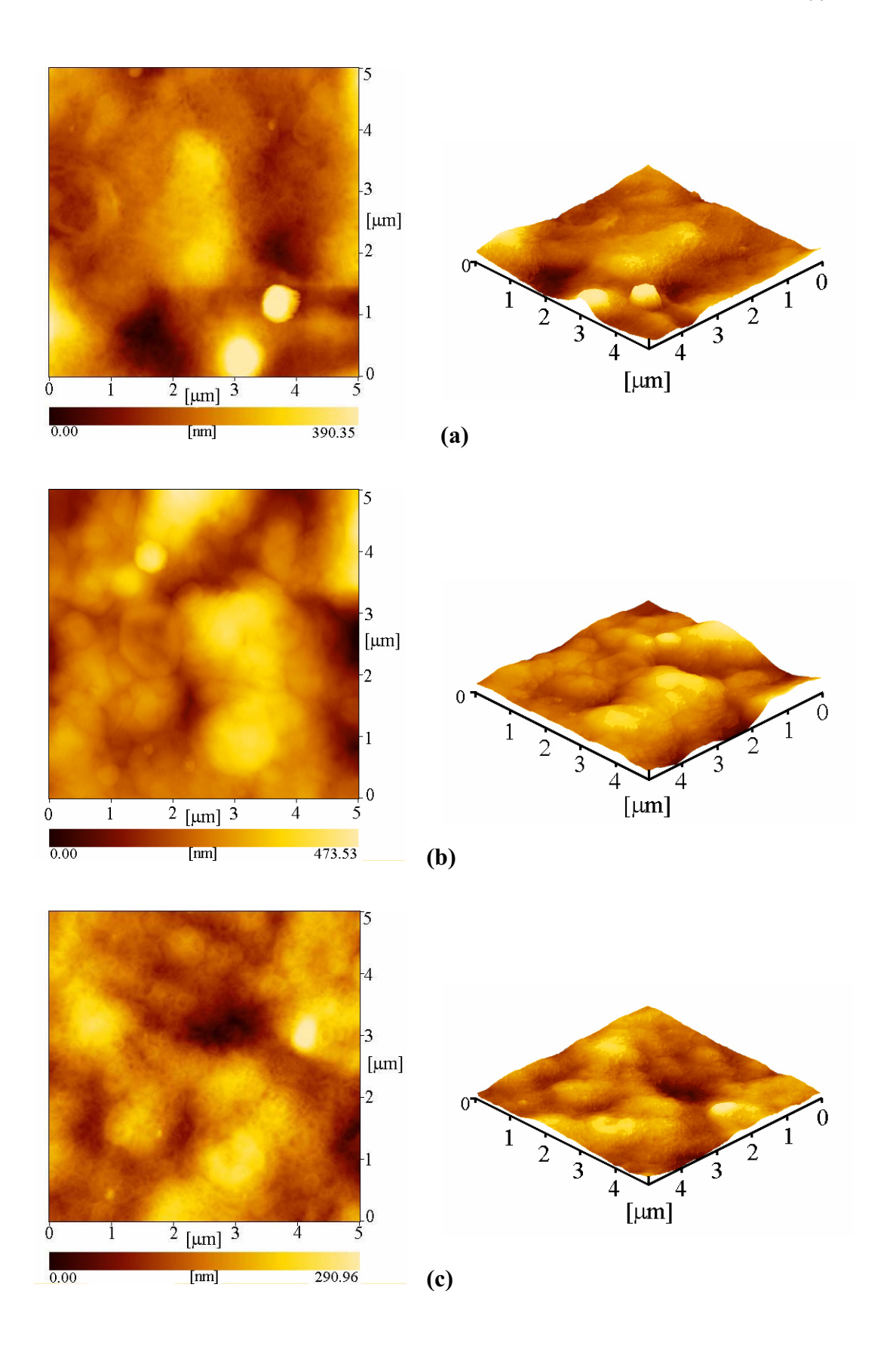


Figure 8. (Ksapabutr et al.)

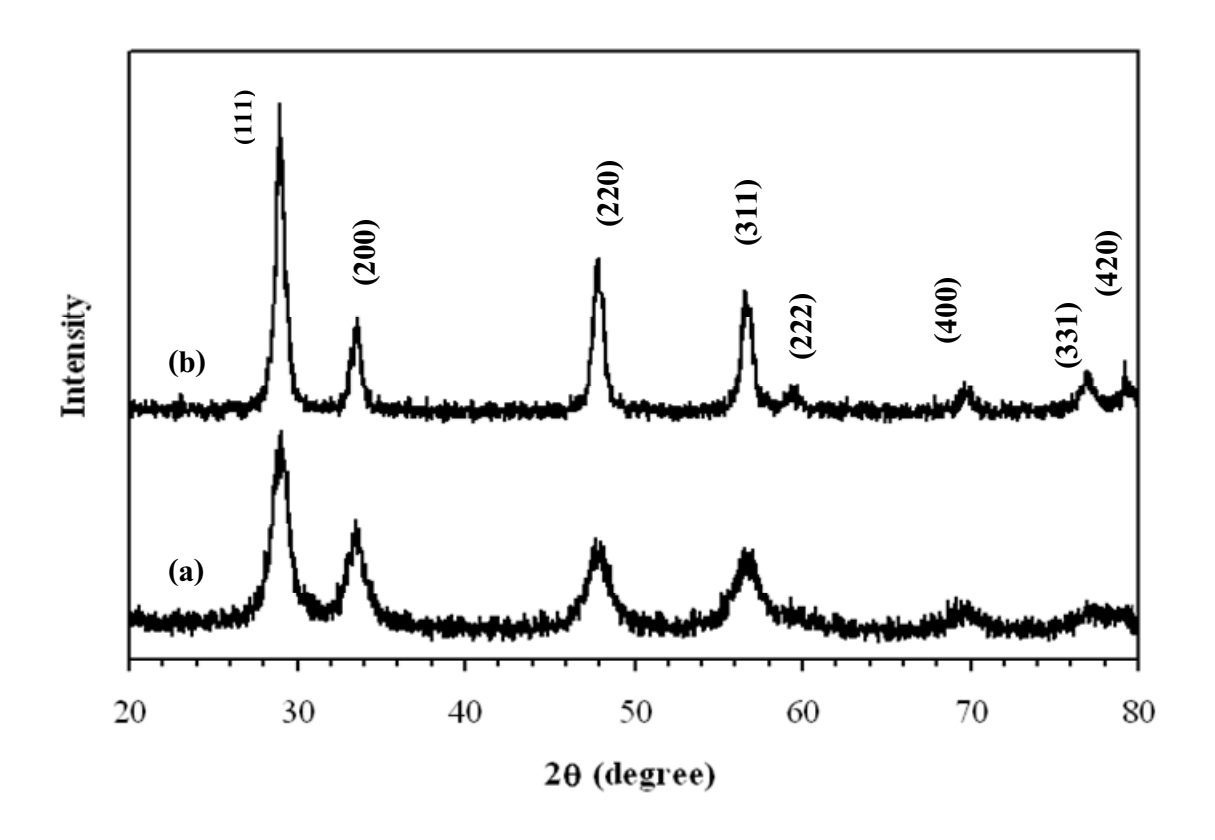


Figure 9. (Ksapabutr et al.)

## ภาคผนวก ข.2

Electrostatic spray deposition of samarium-doped ceria electrolyte coatings
(Submitted to Surface and Coatings Technology)

### Electrostatic spray deposition of samarium-doped ceria electrolyte coatings

Bussarin Ksapabutr <sup>a,\*</sup>, Tanapol Chalermkiti <sup>a</sup>, Sujitra Wongkasemjit <sup>b</sup> and Manop Panapoy <sup>a</sup>

<sup>a</sup> Department of Materials Science and Engineering, Faculty of Engineering and Industrial Technology, Silpakorn University, Sanamchandra Palace Campus, Nakorn Pathom 73000, Thailand.

<sup>b</sup> The Petroleum and Petrochemical College, Chulalongkorn University,

Bangkok 10330, Thailand

#### **Abstract**

Crack-free and dense thin film electrolyte coatings for solid oxide fuel cells by a low-cost and versatile method were investigated. Electrostatic spray deposition (ESD) technique was employed to fabricate samarium doped ceria (SDC) thin film on glass substrate. The different processing parameters were performed to elucidate the influences of the deposition temperature, the nozzle-to-substrate distance and the post-deposition thermal process on the ESD-coated films. The coating morphology and thickness of the resulting films were revealed by scanning electron microscopy (SEM). Chemical compositions were achieved by energy dispersive spectroscopy (EDX). Nanocrystalline structural and roughness investigations of the coatings were realized by X-ray diffraction (XRD) and atomic force microscopy (AFM), respectively. These studies indicated the formation of single-phase SDC films, at low deposition temperature of 300°C. By using the optimized conditions of deposition, the

formation of crack-free and dense SDC thin films with a uniform coverage having

thicknesses less than 400 nm were obtained.

**PACS:** 68.37.-d, 68.55.-a, 81.07. Bc, 81.15 Rs.

**Keywords:** Electrostatic spray deposition; Samarium doped ceria; Thin film coating;

Solid oxide fuel cells

\*Corresponding author. Tel.: +66 34 219 363; Fax: +66 34 219 363.

E-mail address: bussarin@su.ac.th (B. Ksapabutr)

1. Introduction

Solid oxide fuel cells (SOFCs) have many attractive advantages, such as

highly efficient cogeneration for producing electricity and heat, fuel flexibility

(hydrocarbons or nature gas), a wide variety of applications from small-scale to large-

scale power systems and an environmentally friendly technology. In general,

conventional SOFCs require the operating temperatures above 900°C due to low

oxygen ionic conductivity of traditional yttria stabilized zirconia (YSZ) electrolyte [1-

3]. Recently, samarium doped ceria (SDC) materials has become one of the most

important electrolyte materials for intermediate temperature solid oxide fuel cells (IT-

SOFCs) owing to their high oxygen ionic conductivity at low temperature [4-6]. SDC-

based SOFCs can be operated at temperature as low as 400°C when using hydrogen as

the fuel [7]. The decrease of the operating temperature of SOFCs from 900-1000°C to

below 600°C would provide a number of benefits, including cell performance

stability, higher thermodynamic efficiency, lower fabrication cost and cheaper

utilization of stainless steel interconnects [8-9]. These are crucial advantages in the

push to develop commercially viable fuel cells.

Besides alternative electrolyte materials with higher oxygen ionic conductivity, the reduction of dense electrolyte thickness can also improve the performance of IT-SOFCs by decreasing the path for oxygen ions, leading to less ohmic resistance at intermediate temperature (below 600°C) than thicker films at above 900°C. Therefore, the development of thin film technique for IT-SOFCs is motivated by this requirement. Several techniques are available to fabricate thin films, including plasma coating [10], laser deposition [11], chemical vapor deposition [12], or flame-assisted vapor deposition [13], RF magnetron sputtering [14] and electrostatic spray deposition (ESD) [15]. Electrostatic spray deposition is promising in addressing the deposition of thin films because of non-vacuum deposition condition, no usage of sophisticated reactor, a cost-effective deposition with simple setup, inexpensive and non-toxic precursors, easy control of substrate temperature, and defect reparation [16-18].

To the best of our knowledge, the fabrication of SDC thin films using electrostatic spray deposition has not yet been reported. Hence, the preparation of SDC thin films as function of processing parameters was investigated. The deposition temperature, the distance between the nozzle and the substrate and the post-deposition heat treatment are optimized to achieve the dense and uniform thin films with crack-free surface. The phase analysis, microstructure, thickness, roughness of the resulting thin films will be discussed.

# 2. Experimental

### 2.1 Precursor preparation

Stoichiometric amount of samarium nitrate hexahydrate (Sm(NO<sub>3</sub>)<sub>3</sub>.6H<sub>2</sub>O, 99.99 % purity, Aldrich Chemical) and cerium nitrate hexahydrate (Ce(NO<sub>3</sub>)<sub>3</sub>.6H<sub>2</sub>O,

99.99 % purity, Aldrich Chemical) were employed to prepare the precursor solution for  $Sm_{0.1}Ce_{0.9}O_{1.95}$  thin films using ethanol ( $C_2H_5OH$ , 99 % purity, Fluka) as solvent. The concentration of precursor solution was kept constant at 0.02 M.

## 2.2 SDC film fabrication

SDC film was deposited on the top of the glass substrate using electrostatic spray deposition system, as schematically illustrated in Fig. 1. The substrates were cleaned ultrasonically in ethanol prior to deposition. The precursor solution was delivered through a silicone tube to the apex of nozzle by a peristaltic pump (Watson Marlow, 101U/R) at a flow rate of 0.84 ml h<sup>-1</sup>. The stainless steel capillary tube (inner diameter: 0.394 mm, outer diameter: 0.711 mm) with a tilted angle of 15° at the end was used for the capillary nozzle. While high DC electric potential was applied to the precursor solution, electrostatic field was generated between capillary nozzle and grounded substrate, resulting in the atomization of liquid solution into charged droplets. The charged droplets of the precursor solution were then sprayed towards the heated substrate. In this present work, the distance between the tip of the nozzle and the substrate was varied from 7 to 13 cm with an interval of 2 cm. The substrate temperature was varied in the range between 300 and 500°C. In all the experiments, the applied voltage was maintained at a constant value of 15 kV. All films were deposited for 2 h under ambient atmosphere. Afterwards, the bi-layers were annealed at 600 and 700°C in the furnace for 2 h to ensure the development of the crystallinity. The maximum temperature was controlled at 700°C because the glass substrate can be heated without softening at this temperature. Furthermore, the deposition parameters were optimized to produce uniform and dense electrolyte thin films with crack-free. The deposition conditions used in this study were summarized in Table 1.

#### 2.3 Characterization

Characterization of the thermal behavior of the precursor solution was achieved by thermogravimetric analysis (Perkin Elmer, TGA7) with a ramp rate of 5°C min<sup>-1</sup> in an air atmosphere. Changes in temperature at various distances beyond the surface of the substrate were measured using infrared temperature measuring instrument with close focus optics (TESTO 830-T3). The measurement of voltage and electric current at different distances between the nozzle and the substrate was carried out using high voltage test probe (Digicon, HV-40) positioned above the substrate surface about 1 mm and electrometer/high-resistance meter (Keithley Model 6517A). The surface morphology and thickness of the resulting SDC films were observed using a Hitachi S3400N scanning electron microscope, operated at 20 kV, equipped with an energy-dispersive spectroscope (EDS) also used for chemical composition measurements. The structural features and roughness of the coatings were assessed by X-ray diffractometer (XRD, Model Rigaku D/Max 2000HV) with Cu Kα radiation and atomic force microscope (AFM, Seiko, SPI 400 DMF mode), respectively. Moreover, the influence of deposition temperature and the heat treatment process on the development of crystallinity was also examined.

### 3. Results and discussion

Thermogravimetric analysis was performed to find out the minimum deposition temperature required for preparing SDC-based films. Fig. 2 demonstrates the TG and differential TG (DTG) traces of precursor solution. The results revealed the weight losses below 300°C, which corresponded to the evaporation of solvent and

the decomposition of nitrate in precursor solution [19]. Hence, the beginning substrate temperature investigated was 300°C.

SDC films deposited at various substrate temperatures and post-deposition heat-treated were examined by XRD technique. Fig. 3 illustrates the XRD patterns of as-deposited SDC films at different substrate temperatures and post-deposition annealed SDC films at 600 and 700°C. These films were all in the single cubic structure and the diffraction intensity and numbers of peaks corresponding to the SDC phase were enhanced with increasing substrate temperature. The observed diffraction peaks with  $2\theta$  values of 28.76, 33.24, 47.62, 56.48, 59.40, 69.60, 76.74, 79.04 and 88.58 degree can be assigned for the SDC cubic fluorite phase with the planes (1 1 1), (2 0 0), (2 2 0), (3 1 1), (2 2 2), (4 0 0), (3 3 1), (4 2 0) and (4 2 2), respectively. It can be seen that all films have the most preferentially oriented crystal plane of (1 1 1). The line broadening method was used to determine the average size of SDC crystallites for the (1 1 1) peaks, according to the Debye-Scherrer formula [20]. The crystallite size of SDC films as a function of substrate temperature was displayed in Fig. 4. The higher the substrate temperature of substrate, the larger the crystallite size was. With the investigation of post-deposition thermal treatment, we also found that the crystallite size for the as-deposited film at 450°C increased from 8.7 nm to 11.4 and 12.9 nm after heat treatment at 600 and 700°C, respectively.

In order to evaluate the composition of the resultant SDC films, sample surface was investigated by energy dispersive X-ray analysis. The values obtained were presented as arithmetic means of the measurement on 10 specimens (at least twelve points on each observed film). The atomic ratio of Ce:Sm was found out to be 0.87:0.13, which is in good agreement with that of the precursor solution (0.90:0.10). Therefore, the formation of stoichiometric  $Sm_{0.1}Ce_{0.9}O_{1.95}$  films was achieved.

Morphology of the as-deposited SDC thin films at different deposition temperatures and different nozzle-to-substrate distances was elucidated. Table 2 shows the SEM micrographs of SDC thin films fabricated at various substrate temperatures for four different nozzle-to-substrate distances. For deposition temperature ranging from 300 to 500°C, it is found that the crack-surface roughness of the films decreased with increasing substrate temperature up to 450°C. The film deposited at the substrate temperature of 450°C was uniform, dense and crack-free. Consequently, this temperature is considered as the optimal deposition temperature. At the substrate temperature of 500°C, the deposited film showed the granular features. This may be explained that the charged droplets were atomized under the electric field onto the heated substrate, leading to the formation of film due to the vaporization of solvent and the decomposition of precursor solution. Fig. 5 depicts a plot of the change in air temperature as a function of the distance between the nozzle and the substrate (the substrate surface at origin point). Each data point represented the statistical average of at least five individual values. The air temperatures remained almost constant during spraying from nozzle to substrate until a drastic rise in temperature was detected in the vicinity of heated substrate surface. The air temperature started to increase slightly at a distance of approximately 11, 15, 16 and 20 mm away from the substrate surface for the substrate temperature of 300, 400, 450 and 500°C, respectively. It can be seen that at all substrate temperatures, the vaporization of solvent can take place both before and after the charged droplets reached the heated substrate. Clearly, an increase in the substrate temperature will enhance the vaporization rate of the solvent. Moreover, the higher the substrate temperature, the higher the precursor decomposition will be. The majority of the decomposition of precursor takes place in the region close to the heated substrate surface, especially at a low temperature (300°C). This observation is also consistent with the thermal analysis result. Hence, at 300°C, the deposited droplets may contain the largest amount of solvent and nitrate salts. The layer is still wet on the top of the film. The solvent will evaporate too fast, leading to drying stresses that caused the film cracking. The lower substrate temperature will result in non-uniform, rough and crack films, until at 450°C a homogeneous layer was deposited with small droplet-like features (Table 2). Furthermore, the evaporation of charged droplets during atomization causes significant changes in droplet sizes. The higher rate of solvent vaporization at higher substrate temperature leads to the reduction in droplet sizes, resulting in smoother and more uniform films. At so high temperature (500°C), the droplets will excessively dry before arriving at the substrate surface, leading to the powder-like agglomerates of particles emerging from the dense underlayer because of low spreading of the droplets (Table 2).

Regarding the influence of the nozzle-to-substrate distance on coating morphology, SEM micrographs revealed that the nozzle-to-substrate distance affected the quality of coating, as displayed in Table 2. For deposition distance ranging from 7 to 13 cm, the number of cracks decreased with increasing the distance between the nozzle and the substrate. Based on this study, the shorter deposition distance causes crack and rough films, while the longer deposition distance causes crack-free and smoother films, especially at higher substrate temperature. At a largest nozzle-to-substrate distance of 13 cm, most films were crack-free. It might be because a longer distance allowed precursor solution to have more chance to evaporate and decompose during the transport of droplets from the nozzle to the substrate. As stated above, the evaporation also leads to a decrease in droplet size, which results in smaller agglomeration on the top of the dense bottom layers at longer deposition distance.

However, for deposition distance of 13 cm deposited at 500°C, the film roughness increased again compared to the deposition at shorter distance at 500°C. It might be due to lower spreading of droplets when impinging at the substrate surface. The nozzle-to-substrate distance not only affected the path length of charged droplets, but also the electrical field strength. The results from the measurement of voltage and electric current above the surface of the substrate about 1 mm suggest that the voltage and electric current at near the substrate surface decreased with an increase of the distance between the nozzle and the substrate, as shown in Fig. 6. Furthermore, it was found that the measured voltage and electric current during spraying were lower than those recorded without the atomization of precursor solution, especially at the nozzle-to-substrate distance ranging from 9 to 15 cm. The diminution of voltage and current causes a decrease of electric field strength, which results in the reduction of charged droplet velocity. Therefore, the enhancement of solvent vaporization and precursor decomposition can be attained.

Fig. 7 presents the cross-section of SDC coating deposited at different nozzle-to-substrate distances at 450°C onto glass substrate after a deposition time of 2 h. It can be clearly seen that the coating on top of the glass substrate consists of a dense top layer. The coating thickness decreased with increasing the nozzle-to-substrate distance owing to the lower droplet number density near the substrate surface. This result can be confirmed by the investigation of the spray pattern at the substrate. Precursor solution was sprayed onto substrate at 450°C with a flow rate of 0.84 ml h<sup>-1</sup> under high voltage of 15 kV by varying the distance between the nozzle and the substrate (see photographs in Fig. 8). The deposition area of some films deposited at 5, 7 and 9 cm on the substrate can be determined by means of Simpson's rule [21]. It is found that the deposition area increased with increasing the nozzle-to-substrate

distance (see lines in Fig. 8). In other words, a larger deposition area was obtained when the same quantity of precursor solution was atomized over the same substrate at larger distances between the nozzle and the substrate, leading to a decrease in film thickness. The resultant film thicknesses were about 2.28  $\mu$ m, 1.21  $\mu$ m, 532 nm and 370 nm at the nozzle-to-substrate distance of 7, 9, 11 and 13 cm, respectively.

The atomic force microscopy (AFM) images in Fig. 9 exhibit the surface topography of the as-deposited thin films on the glass substrate fabricated at 450°C at the nozzle-to-substrate distances of 11 and 13 cm. These two deposition distances at 450°C were only investigated the roughness of as-deposited SDC films because they show the highest smooth-surface, as shown in Table 2. In order to find out the optimal deposition conditions, the root mean square (RMS) surface roughness of both films was clarified. The film deposited at the distance of 13 cm was found to be rougher (RMS = 102.1 nm) than that deposited at the distance of 11 cm (RMS = 53.7 nm). At the deposition distance of 13 cm and the substrate temperature of 450°C, the rate of the solvent vaporization and the salt decomposition is too high when compared to condition at deposition distance of 11 cm, indicating an increased surface roughness.

To investigate the effect of the post-deposition heat treatment process on the morphology of SDC films, the films deposited at various deposition temperatures were further heat-treated at 700°C. Table 3 displays SEM micrographs of the films deposited at different substrate temperatures after annealing at 700°C. It is notable that the formation of the cracked layer increased after heat treatment of film deposited at 300°C at the deposition distances of 7, 9 and 11 cm. It clearly indicated that the decomposition of nitrate salt and the vaporization of solvent in the spray droplets did not take place completely before reaching the substrate surface. This morphology is always found to be present at low deposition temperature and short deposition

distance. At all nozzle-to-substrate distances, smoother films were obtained when the deposition temperature increased. It may be due to the reduction of stress residual from the impact of charged droplets on substrate. As mentioned above, two deposition distances at 450°C were investigated the roughness of as-deposited SDC films due to the highest smooth- surface compared to other conditions. Fig. 10 represents AFM images of the thin films at the nozzle-to-substrate distances of 11 and 13 cm deposited at 450°C after heat treatment at 700°C. Root mean square (RMS) surface roughness of the films after annealing was smaller than those before annealing. Additionally, the heat-treated film deposited at the distance of 13 cm was also found to be rougher (RMS = 64.2 nm) than that deposited at the distance of 11 cm (RMS = 10.1 nm).

Conclusively, smooth and dense films with crack-free can be fabricated over a wide range of deposition conditions. Both substrate temperature and nozzle-to-substrate distance are the critical deposition parameters controlling the morphology of the films. The low densification temperature prevents the excessive grain growth, and makes it easy to obtain nanocrystalline SDC films. Moreover, the low temperature processing of nanocrystalline SDC films is beneficial to practical applications; it allows the deposition of dense SDC or/and other ceria-based films with saving energy cost. In this work, the substrate temperature of 450°C and the nozzle-to-substrate distance of 11 cm are the optimal deposition conditions to achieve the highest smooth and dense films with crack-free for as-deposited coating. In addition, the highest smoothness of dense and crack-free thin films can be achieved after thermal treatment at 700°C of film deposited at the substrate temperature of 450°C and the deposition distance of 11 cm.

#### 4. Conclusions

Dense thin films of SDC with a nominal composition of Sm<sub>0.1</sub>Ce<sub>0.9</sub>O<sub>1.95</sub> have been successfully deposited on glass substrate by a simple and efficient ESD technique using starting materials of samarium nitrate and cerium nitrate in ethanol. The cubic phase of nanocrystalline SDC films was obtained at a relatively low temperature deposition at 300°C. The optimal ESD processing parameters, including deposition temperature, nozzle-to-substrate distance and post-deposition heat treatment were elucidated. The deposition temperature and the distance between the nozzle and the substrate are directly correlated with each other due to their influences on the vaporization of solvent, the decomposition of precursor solution and the droplet size. The effectiveness of ESD-coating can be increased by adjusting the processing parameters to fabricate dense thin films with crack-free surface. Optimal conditions for the fabrication of the most uniform, smooth, dense and single phase SDC films with crack-free by ESD technique were considered to be at the substrate temperature of 450°C and the deposition distance of 11 cm both before and after thermal treatment at 700°C.

### 5. Acknowledgments

The authors are grateful to the following financial supports: Thailand Research Fund (TRF); The Commission of Higher Education; Department of Materials Science and Engineering, Faculty of Engineering and Industrial Technology, Silpakorn University.

#### 6. References

- 1. Y. Zhang, J. Gao, D. Peng, M. Guangyao, X, Liu, Ceram. Int. 30 (2004) 1049.
- 2. W. Bao, W. Zhu, G. Zhu, J. Gao, G. Meng, Solid State Ionics 176 (2005) 669.

- S. Lee, Y. Lim, E. A Lee, H. J. Hwang, J.W. Moon, J. Power Sources 157 (2006) 848.
- 4. W. Huang, P. Shuk, M. Greenblatt, Solid State Ionics 100 (1997) 23.
- 5. J. G. Li, T. Ikegami, T. Mori, Acta Mater. 52 (2004) 2221.
- H. H Huang, H. P. Chang, Y. T. Chien, M. C.Huang, J. S. Wang, J. Cryst. Growth 287 (2006) 458.
- C. Lu, W. L. Worrell, R. J. Gorte, J. M. Vohsb, J. Electrochem. Soc. 150(3) (2003) A354.
- 8. S. Ohara, R. Maric, X. Zhang, K. Mukai, T. Fukui, H. Yoshida, T. Inagaki, K. Miura, J. Power Sources 86 (2000) 455.
- 9. A. B. Stambouli, E. Traversa, Renew. Sust. Energ. Rev. 6 (2002) 433.
- H. B. Wang, J. F. Gao, D. K. Peng, G. Y. Meng, Mater. Chem. Phys. 72 (2001)
   297.
- 11. X. Han, G. Wang, J. Jie, X. Zhu, J.G. Hou, Thin Solid Films 491 (2005) 249.
- 12. G.L. Bertrand, G. Caboche, L.C. Dufour, Solid State Ionics 129 (2000) 219.
- 13. K. L. Choy, S. Charojrochkul, B. C. H. Steele, Solid State Ionics 96 (1997) 49.
- X. Zhang, H. Ma, Q. Wang, J. Ma, F. Zong, H. Xiao, F. Ji, S. Hou, Physica B. 364 (2005) 157.
- S. G. Kim, K. H. Choi, J. H. Eun, H. J. Kim, C. S. Hwang, Thin Solid Films 377-378 (2000) 694.
- 16. T. Nguyen, E. Djurado, Solid State Ionics 138 (2001) 191.
- I. Taniguchi, R. C. Van Landschoot, J. Schoonman, Solid State Ionics 160 (2003)
   271.
- Cheng-Yun Fu, Chin-Liang Chang, Ching-Shiung Hsu, Bing-Hwai Hwang,
   Mater. Chem. Phys. 91 (2005) 28.

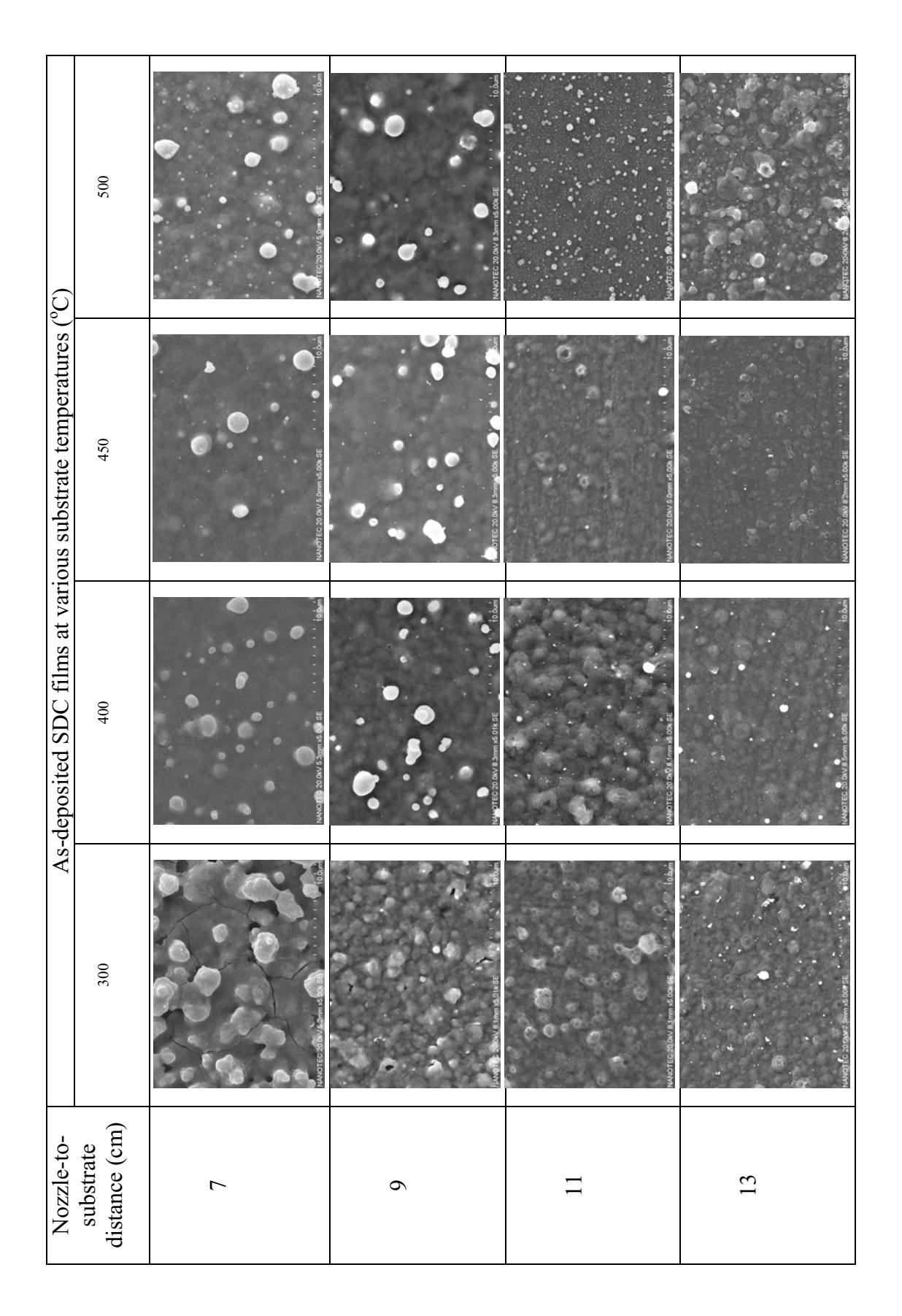
- M. Kamruddin, P.K. Ajikumar, R. Nithya, G. Mangamma, A.K. Tyagi, B. Raj,
   Powder Technol. 161 (2006) 145.
- B.D. Cullity, Elements of X-Ray Diffraction, Addison-Wesley Publication Company, Reading, MA, 1978.
- 21. S.C. Chapra, R.P. Canale, Numerical Methods for Engineers with Programming and Software Applications, McGraw-Hill, Singapore, 1998.

## **Table captions**

- **Table 1.** Deposition and heat treatment conditions employed in this study.
- Table 2. SEM images (magnification = 5000x; scale bar =  $10 \mu m$ ) of as-deposited SDC thin films at different substrate temperatures for four different nozzle-to-substrate distances.
- **Table 3.** SEM images (magnification = 5000x; scale bar =  $10 \mu m$ ) of SDC thin films deposited at different substrate temperatures for four different nozzle-to-substrate distances after heat treatment at  $700^{\circ}$ C.

Applied	Liquid	Precursor	Deposition	Nozzle-to-	Annealing
potential	flow rate	concentration	temperature	substrate	temperature
(kV)	(ml h <sup>-1</sup> )	(M)	(°C)	distance	(°C)
				(cm)	
15	0.86	0.02	300	7	600
			400	9	700
			450	11	
			500	13	

Table 1. (Ksapabutr et al)



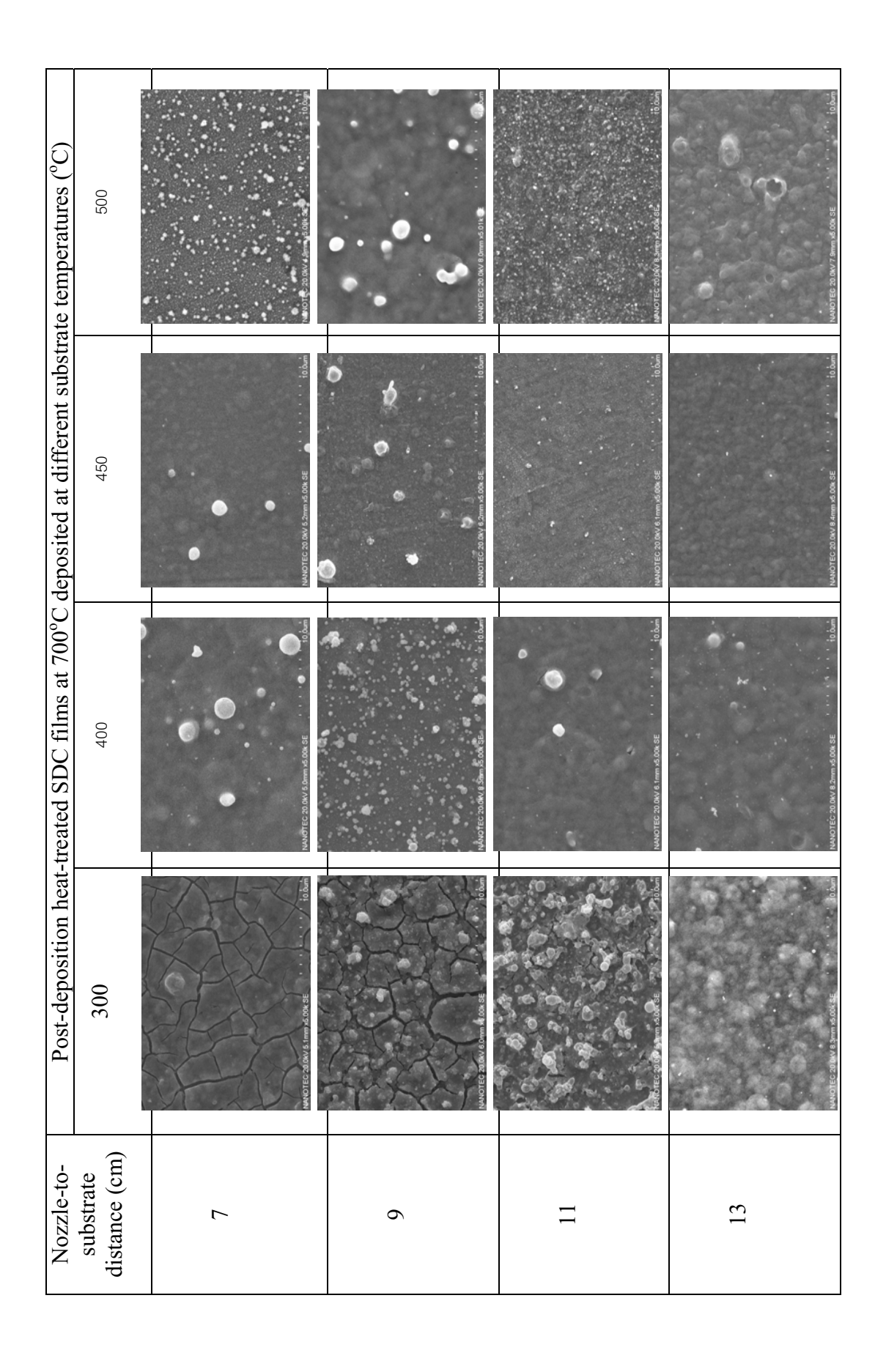


### Figure captions

- Figure 1. Schematic diagram illustrating the electrostatic spray deposition setup used in this work: (1) High voltage generator, (2) Peristaltic pump, (3) Temperature controller, (4) Electrometer, (5) Heating element, (6) K-type thermocouple, (7) Extended probe, (8) High voltage test probe, (9) Substrate, (10) Nozzle.
- Figure 2. TG/DTG curves of SDC precursor solution.
- **Figure 3.** XRD patterns of as-deposited SDC films at various substrate temperatures and post-deposition heat-treated SDC films at 600 and 700°C.
- **Figure 4.** The crystallite size of SDC films as a function of substrate temperature and annealing temperature.
- **Figure 5.** Temperature variations between the nozzle and the substrate surface (inset: a detail of low distance range).
- **Figure 6.** Influence of nozzle-to-substrate distance on (a) voltage and current, (b) electric field strength.
- **Figure 7.** Cross-section SEM micrographs of SDC coating deposited at various nozzle-to-substrate distances on the top of glass substrate after 2 h of deposition at 450°C.
- **Figure 8.** Deposition area and photographs of deposition distribution as a function of nozzle-to-substrate distance at the substrate temperature of 450°C.
- **Figure 9.** Three and two-dimensional AFM topologies of as-deposited thin films at  $450^{\circ}$ C (a) 11 cm, (b) 13 cm.
- **Figure 10.** Three and two-dimensional AFM topologies of thin films deposited at 450°C and then heat-treated at 700°C (a) 11 cm, (b) 13 cm.

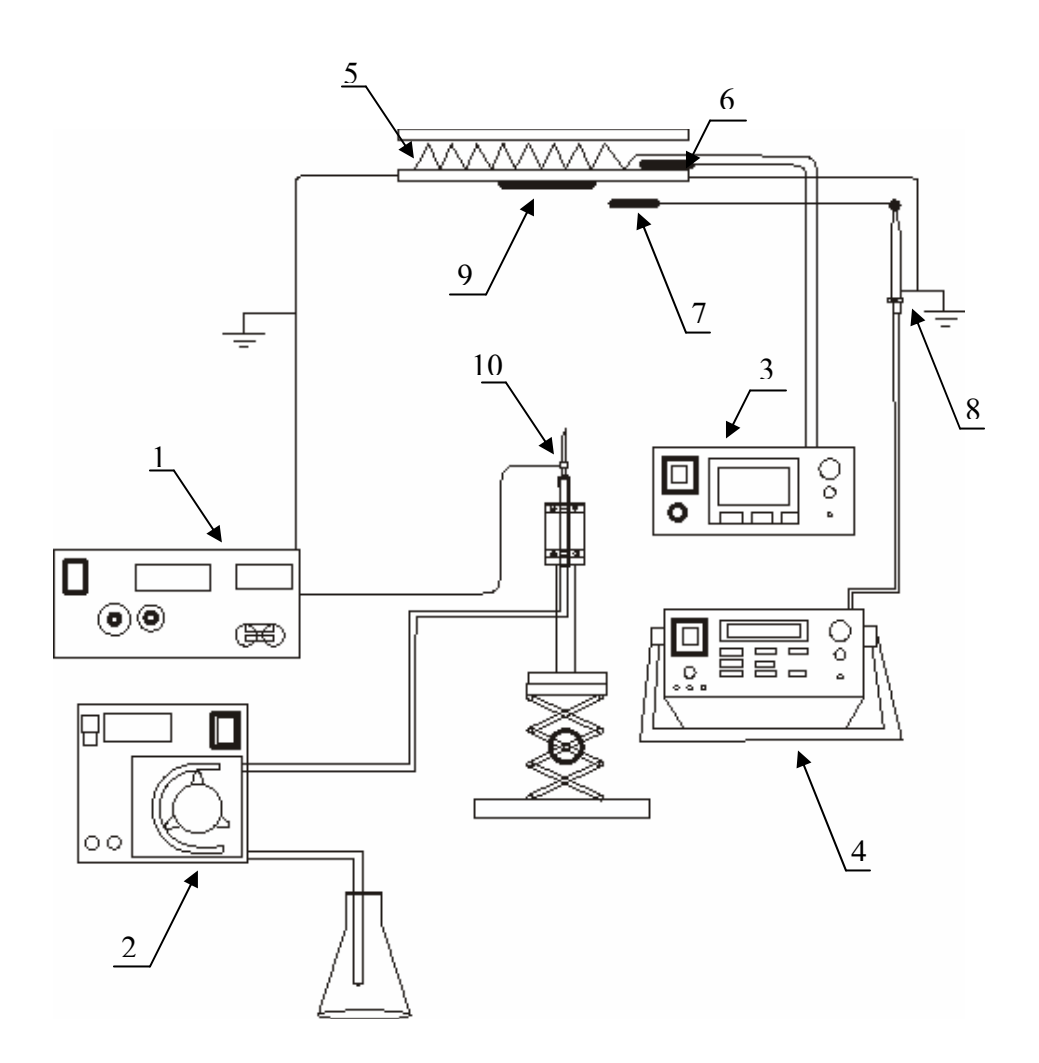


Figure 1. (Ksapabutr et al.)

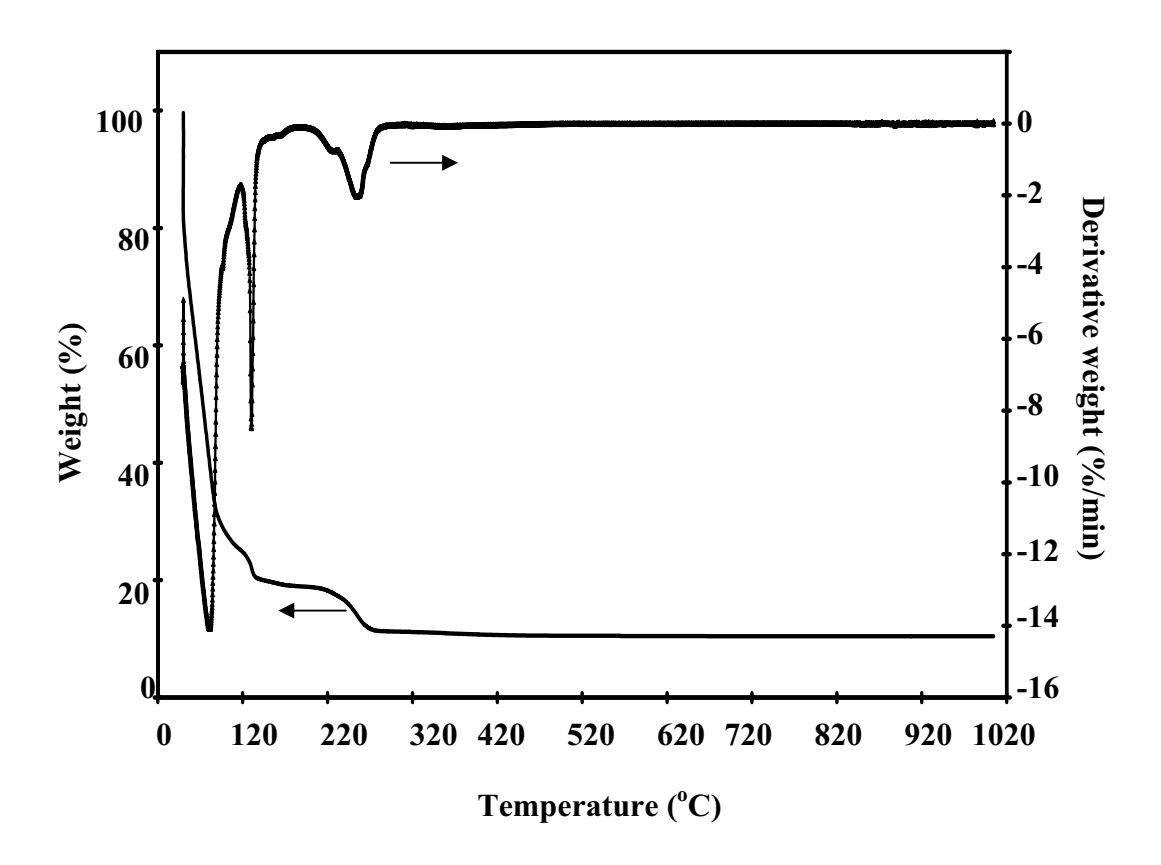


Figure 2. (Ksapabutr et al.)

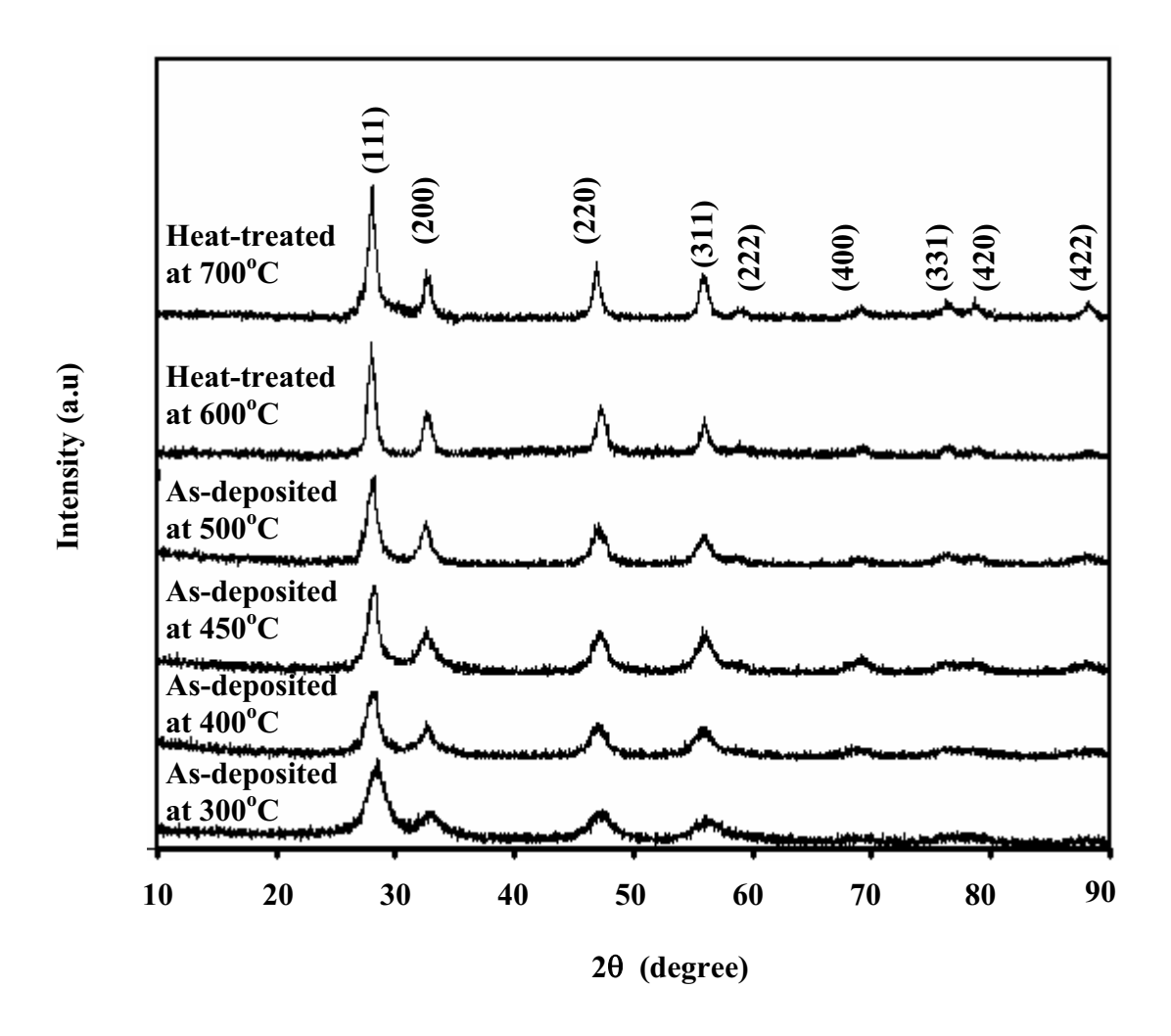


Figure 3. (Ksapabutr et al.)

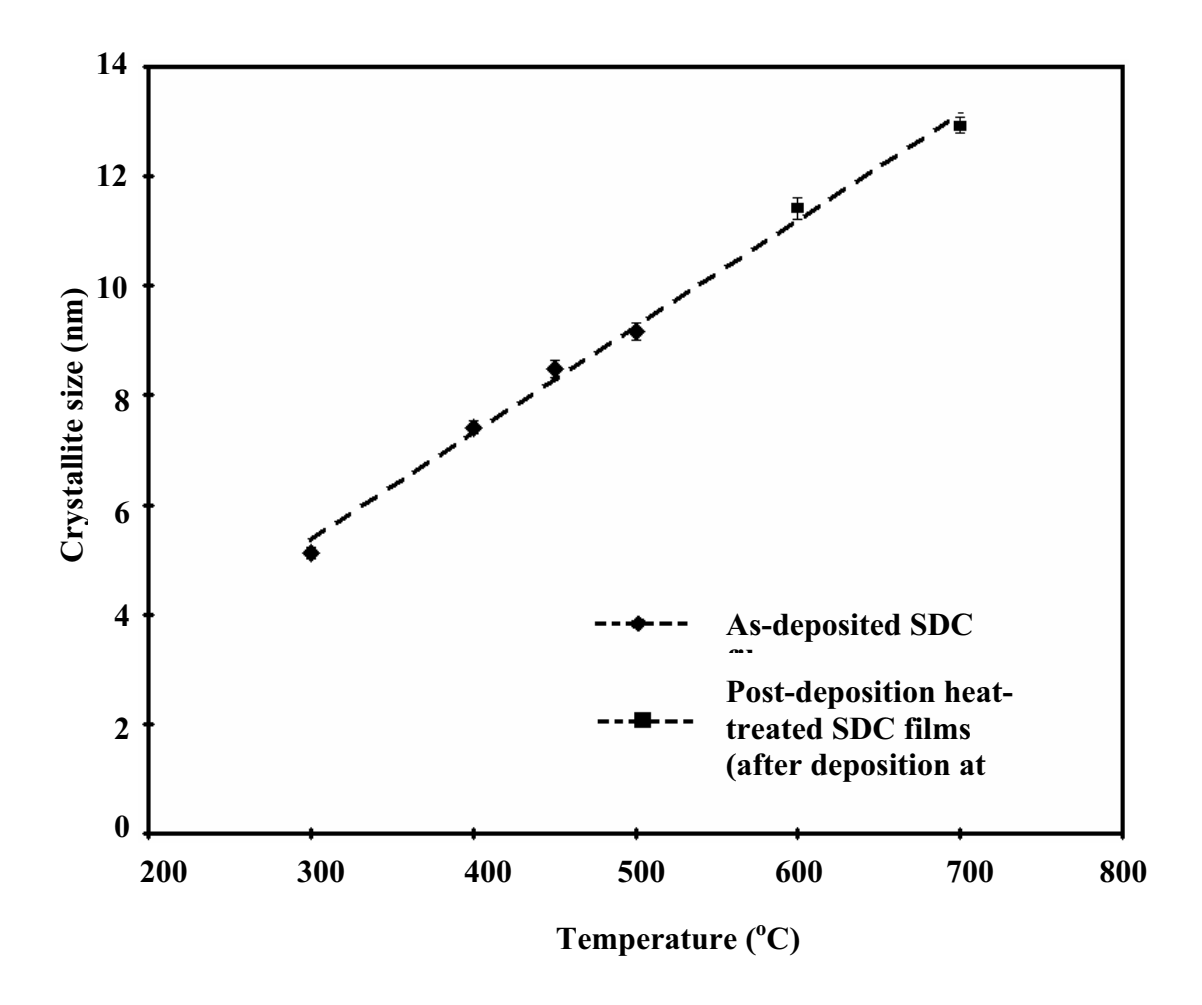


Figure 4. (Ksapabutr et al.)

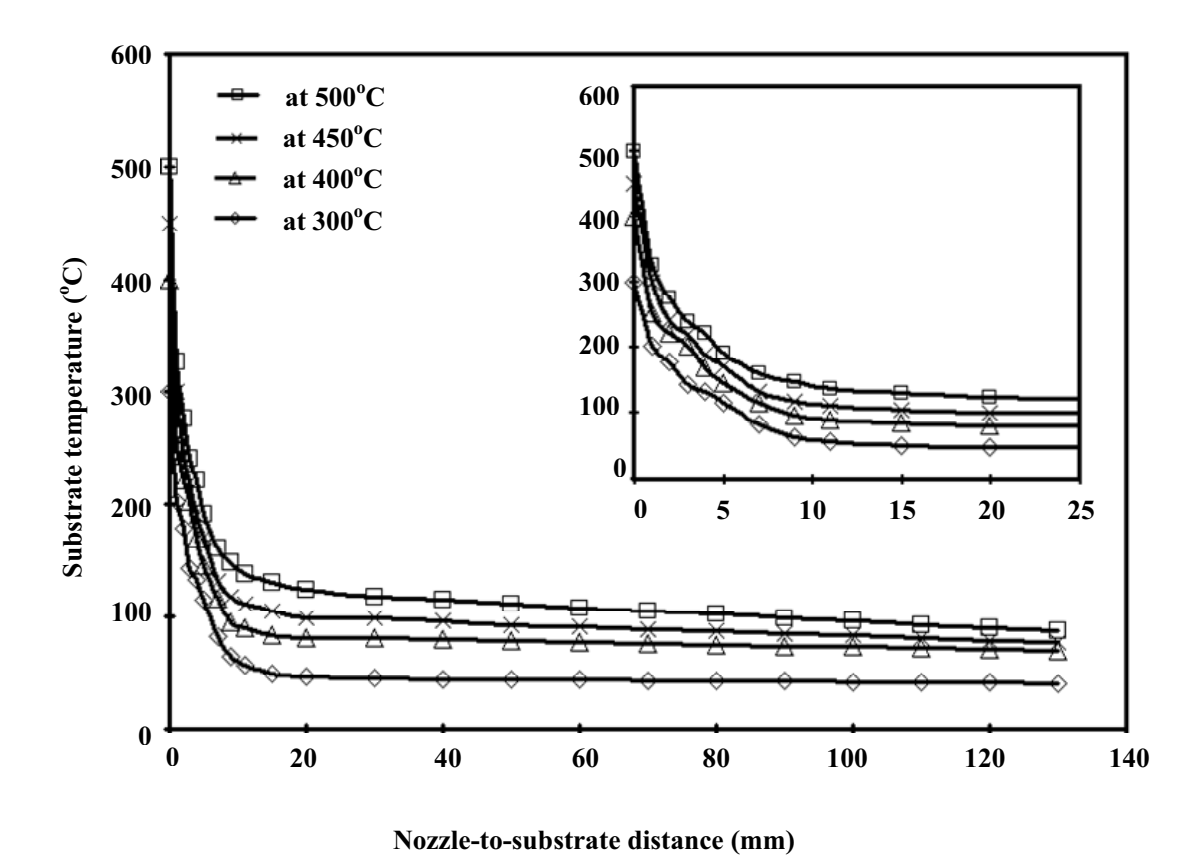


Figure 5. (Ksapabutr et al.)

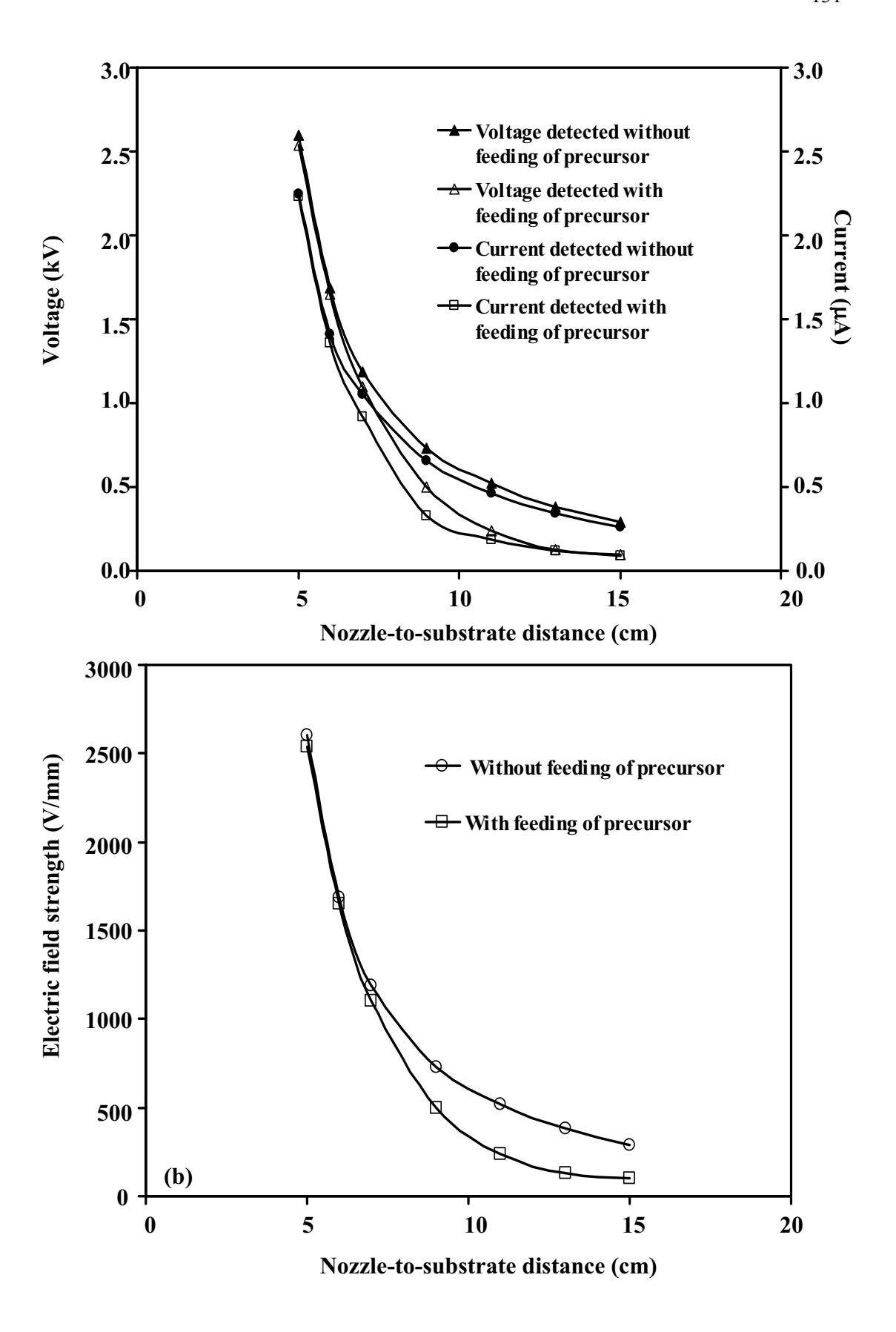
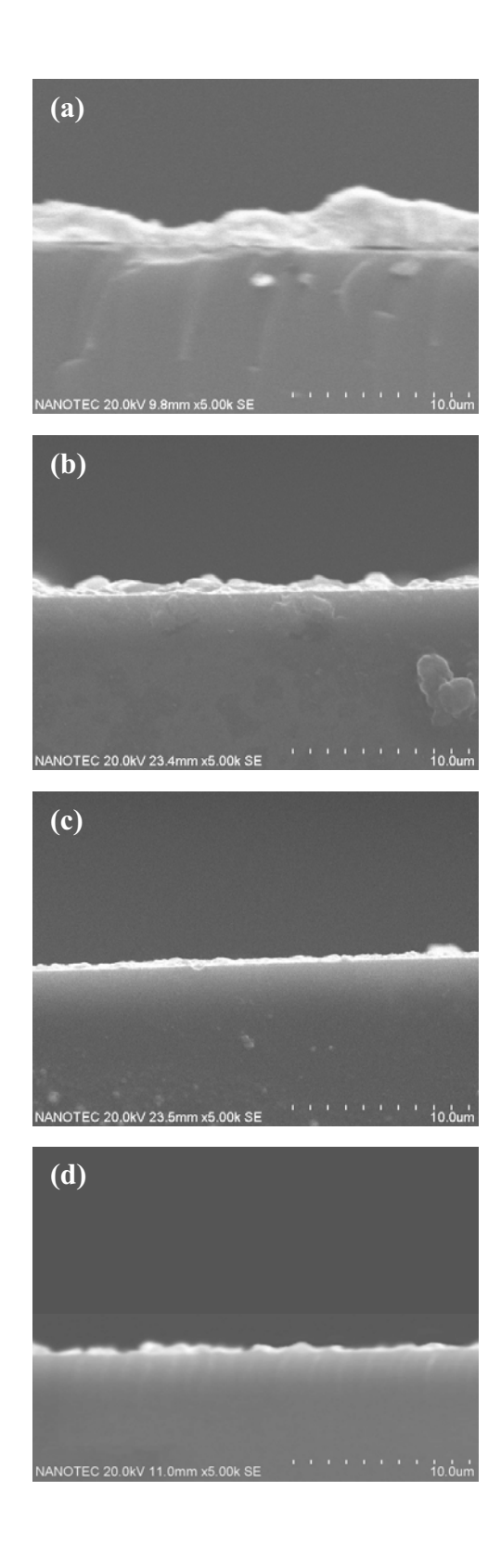


Figure 6. (Ksapabutr et al.)



**Figure 7.** (Ksapabutr et al.)

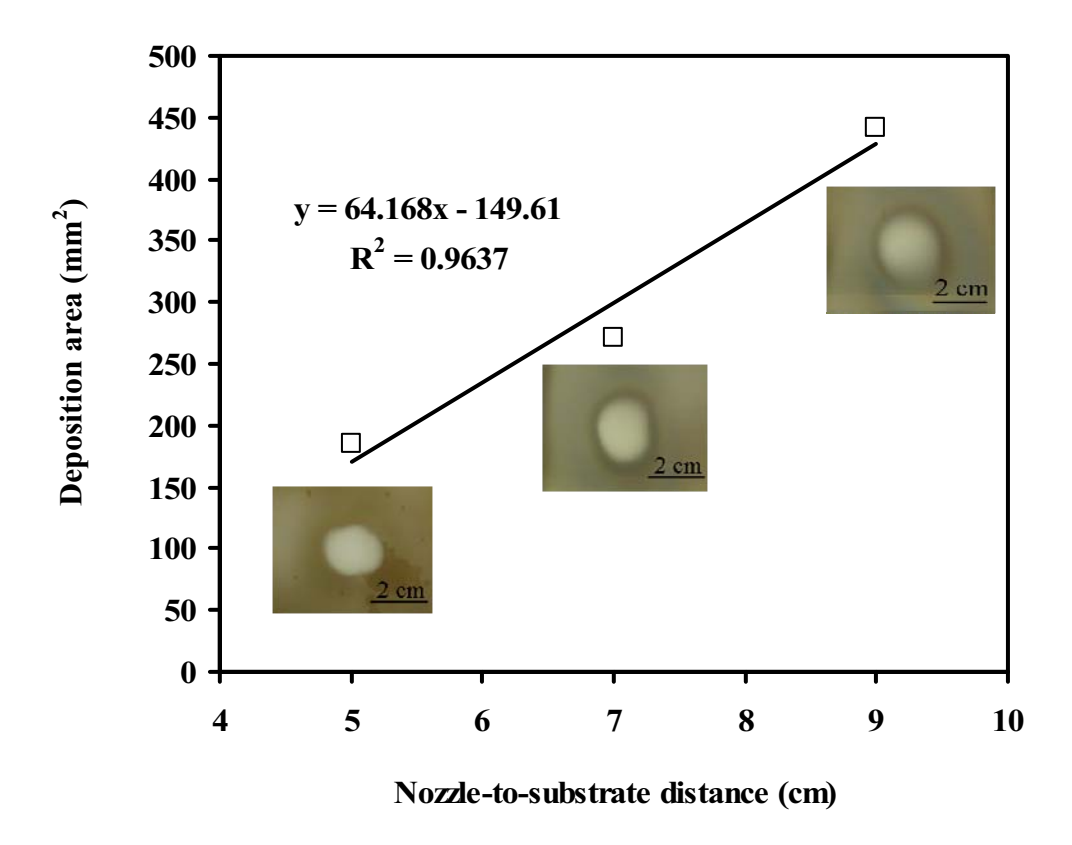


Figure 8. (Ksapabutr et al.)

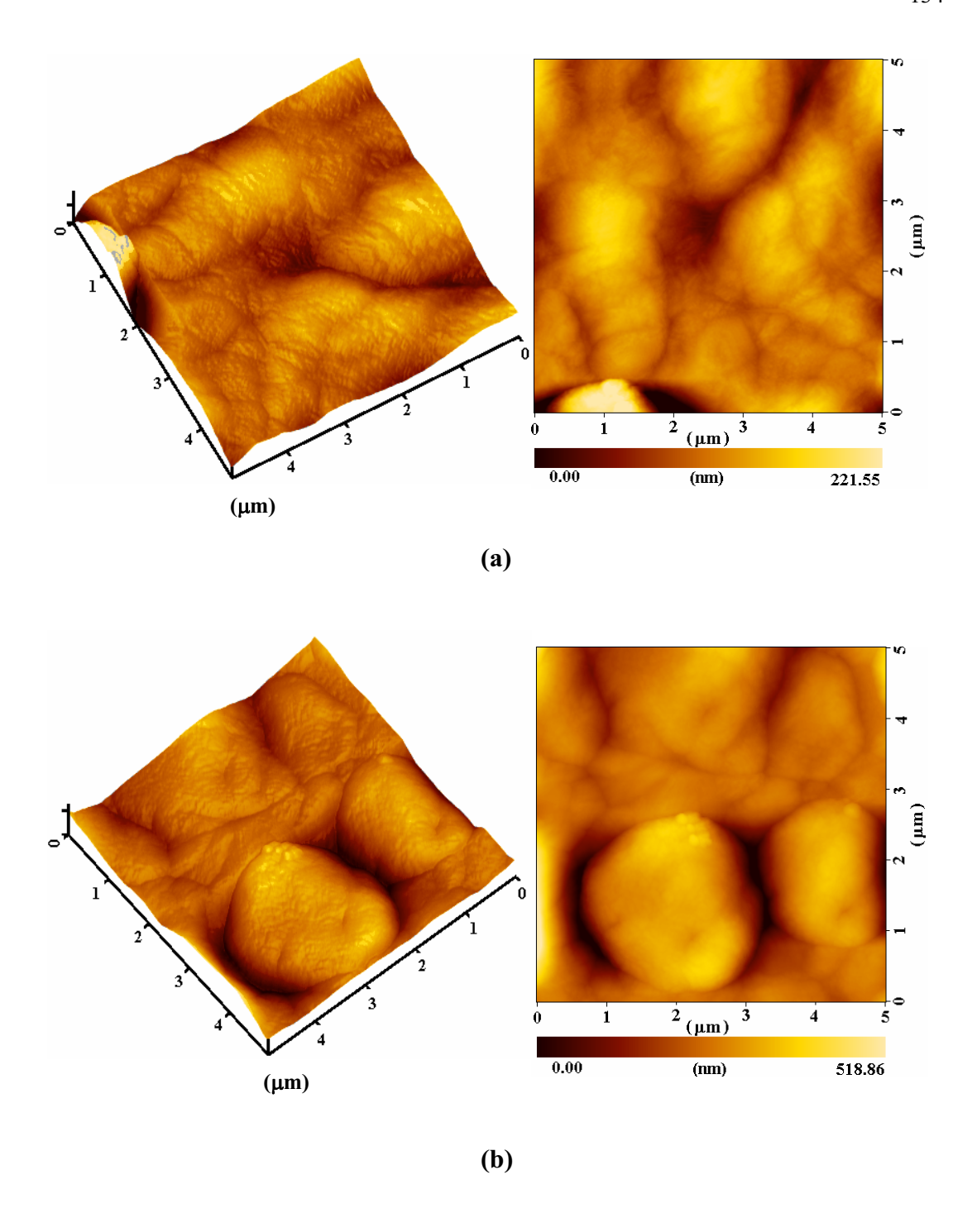


Figure 9. (Ksapabutr et al.)